Journal of the Argentine Chemical Society

NICKEL DEPOSITION ON CERIA: A DFT+U STUDY

Dan Rajsfus[1], Agustín Salcedo[1,2], Brian Milberg[1,2], Beatriz Irigoyen[1,2*]

[1] *Universidad de Buenos Aires. Departamento de Ingeniería Química, Pabellón de Industrias, Ciudad Universitaria, (1428) Buenos Aires, Argentina.*

[2] *CONICET - Universidad de Buenos Aires. Instituto de Tecnologías del Hidrógeno y Energías Sostenibles (ITHES). Buenos Aires, Argentina.*

** Corresponding author. E-mail: beatriz@di.fcen.uba.ar*

Received February 25th, 2017. Accepted in final form May 10th, 2017

Abstract

In this work, we studied the deposition of nickel (Ni) particles and on the (111) surface of CeO_2 (ceria) within a DFT+U framework in order to gain a better understanding of the structural characteristics of Ni/CeO_2 catalysts at atomic level. We examined different geometrical configurations for Ni: isolated (hollow) and in clusters (pyramidal and rhomboidal). Our results show that, for these configurations, there is a strong interaction between Ni and the support, with a charge transference from Ni to ceria. In the case of the Ni_4 clusters, the computed adsorption energy indicates that the rhomboidal configuration is more stable than the pyramidal one. Besides, there is a charge delocalization in the hole between the Ni^{1+} and O^{2-} ions in both Ni_4 configurations.

Resumen

En este trabajo se estudió la deposición de partículas de níquel (Ni) sobre la superficie (111) del CeO_2 (ceria) efectuando cálculos mecano-cuánticos DFT+U, con el objetivo de mejorar la comprensión a nivel atómico de las características estructurales de los catalizadores Ni/CeO_2. Se analizaron diferentes configuraciones geométricas para el Ni: aislado (*hollow*) y formando clústeres (piramidal y romboidal). Nuestros resultados indican que para esas configuraciones existe una fuerte interacción entre la fase activa Ni y el soporte, computándose una transferencia de carga desde el Ni hacia el CeO_2. En cuanto a los clusteres Ni_4, los valores calculados de energía de adsorción indican que la disposición romboidal es más estable que la piramidal. Además, se observa una deslocalización de densidad electrónica en la cavidad entre los iones Ni^{1+} y los aniones O^{2-} en ambas configuraciones.

Palabras Clave: Deposición de níquel; Óxido de cerio; Clusters Ni4; Cálculos DFT+U

Keywords: Nickel deposition; Cerium oxide; Ni4 clusters; DFT+U calculations

1. Introduction

In the current global context, where the growing demand of energy motivates the search of unconventional alternatives, hydrogen could become the main renewable energy source in the future. Molecular hydrogen (H_2) stands out because it can be stored in both liquid and gaseous state, and distributed by pipes [1]. In the long term, H_2 could replace natural gas because it is an environmentally friendly combustible, with an attractive cost [2]. Because of this, different international institutions promote and support the development of new safe and competitive technologies for hydrogen production, in order to satisfy the energetic needs of the growing population [1].

Currently, 95% of the global H_2 production originates from hydrocarbons, while only 4% is obtained from water electrolysis and 1% from biomass. The H_2 production from hydrocarbons has carbon dioxide (CO_2) as a by-product, which is considered the main responsible of greenhouse effect. Right now, the focus is shifting to generating H_2 from primary energy sources as wind, biomass and solar energy, in order to gradually replace the traditional processes [3].

Also, considering that H_2 is mainly obtained from catalytic processes, the design of catalysts with low cost, high activity, and high selectivity is particularly important.

One of the main catalytic processes employed for the production of hydrogen is the Steam Methane Reforming (SMR). Currently, SMR is the most important on an industrial scale; not only for H_2 production but also for syngas (CO e H_2) one, which is widely used for the synthesis of methanol and ammonia [4].

A very important challenge in the design of catalysts for hydrogen production is replacing noble metals as Pt and Rh, with more accessible and economical alternatives that at the same time provide equivalent catalytic performance. Nickel is an abundant and economical transition metal, and is widely used in catalytic processes as alcohols and hydrocarbons reforming reactions. Even though Ni catalyst show a high initial activity, it is rapidly deactivated by carbon deposition [5]. Another factor that affect the performance of Ni is the presence of sulfur in the feed stream. This is because sulfur poisons the catalyst, even in concentrations on the order of parts per billion [6].

Reducible oxides can be used as supports for the metal active phase, as they can either directly participle in the reaction or change the chemical properties of the metal. Historically, alumina (Al_2O_3) was the most common support for Ni-based catalysts [7]. However, CeO_2 (ceria) is an alternative support for Ni of special interest due to its oxygen storage capacity (OSC), which has a key role in improving the resistance of Ni to coke deposition [8–10]. This feature is mainly

attributed to an easy oxygen donation, which is originated by the ability of Ce cation to change its formal oxidation state from Ce^{4+} to Ce^{3+} [11,12]. Besides, CeO_2 can substantially improve the stability and catalytic performance of Ni.

Ceria is commonly used in three-way catalysis (TWC), sulfur oxides removal, preferential oxidation of carbon monoxide (CO-PROX), water-gas shift reaction (WGS) and H_2 production from alcohols and hydrocarbons, among others [13,14].

Previous studies have shown that Ni/CeO_2 catalysts are active and selective for both water-gas shift and steam reforming reactions [15–17]. Despite this, studies at fundamental level of their structure and electronic properties are still scarce in the literature. Therefore, in the present work we present a detailed theoretical study of the Ni/CeO_2 system. This study involved density functional theory (DFT) calculations, that we performed with the Hubbard (U) correction for Ce(4f) orbitals. We examined the metal-support interactions, as well as the changes in geometrical structure and electronic properties of CeO_2 resulting from Ni deposition.

2. Theoretical Methods

Cerium oxide has a fluorite-type cubic structure, with a reported experimental value for its lattice parameter of 5.41 Å [18]. This structure consists of a face-centered cubic (fcc) system of Ce^{4+} cations, with O^{2-} anions filling the tetrahedral voids. We constructed the model of CeO_2 surface by cleaving the optimized bulk cell with the (111) plane and retained an extra oxygen layer. We choose the (111) surface to study Ni deposition because it is the most stable among the low-index (111), (110) and (100) surfaces, and corresponds to minimal Ce–O bonds cleavage [19–21]. Fig. 1 shows a front view of the clean CeO_2(111) surface, where 3 layers can be seen (surface oxygen, Ce and subsurface oxygen).

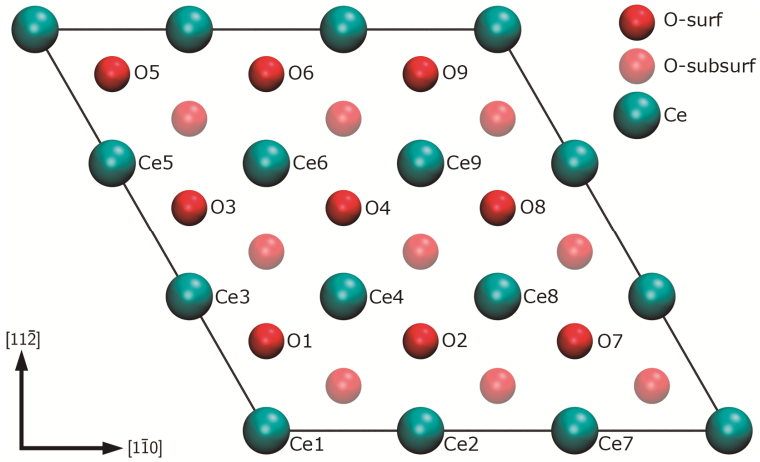

Figure 1. Front view of the CeO_2(111) slab.

First principles calculations were performed within the framework of density functional theory (DFT) as implemented in the Vienna Ab-initio Simulation Package (VASP) [22,23]. The Kohn-Sham equations were solved with the generalized gradient approximation (GGA), and the exchange correlation functional of Perdew-Burke-Ernzerhof (PBE). All calculations are spin-polarized. Geometries were optimized until the Hellmann-Feynman forces had converged to less than 0.02 eV/Å. The cutoff energy of the plane wave basis was set to 500 eV, and the core electrons were represented with the projector augmented wave (PAW) method. We used the Ce($5s^2$, $5p^6$, $6s^2$, $5d^1$, $4f^1$), Ni($3d^8$ $4s^2$) and O($2s^2$, $2p^4$) configurations for valence electrons.

Self-consistent calculations were performed sampling the Brillouin zone with a 3×3×1 k-points grid under the Monkhorst-Pack scheme [24].

The standard DFT formulation usually fails to describe strongly correlated electrons in partially occupied d and f orbitals, due to a deficient treatment of electron correlation. This limitation can be corrected to some extent by using the DFT + U method, where the introduction of a Hubbard 'U' parameter modifies the electron self-interaction error and enhances the description of the correlation effects. Therefore, the value U_{eff} = 5 eV was chosen for the Ce(4f) states as it correctly described the atomic and electronic structure of both CeO_2 and CeO_{2-x} systems [25,26].

Oxidation states and electron occupancy were computed by performing Bader charge and spin charge density analysis [27,28,29].

Nickel adsorption energy ($\Delta E_{ads,Ni}$) on the $CeO_2(111)$ surface was calculated as:

$$\Delta E_{ads,Ni} = E[Ni_y/CeO_2(111)] - E[Ni_y] - E[CeO_2(111)]$$

In this formula, $E[Ni_y/CeO_2(111)]$ represents the computed total energy of the different systems, $E[CeO_2(111)]$ is that of the clean ceria surface, and $E[Ni_y]$ is the corresponding total energy of Ni isolated species (y=1) or Ni_4 clusters in vacuum.

We also evaluated the charge density difference for the two cluster configurations. To make these plots, we calculated the charge density difference matrix (ρ_{diff}) as:

$$\rho_{diff} = \rho[Ni_4/CeO_2(111)] - \rho[Ni_4] - \rho[CeO_2(111)]$$

Here, $\rho[Ni_4/CeO_2(111)]$ is the charge density matrix for the optimized systems after relaxation. Then, we obtained $\rho[CeO_2(111)]$ by performing atomic fixed position calculations for the slab in the exact same post-relaxation geometrical configuration, but without the Ni_4 adsorbate. The opposite was done to obtain $\rho[Ni_4]$.

3. Results and Discussion

In this work, we studied the deposition of nickel particles on the $CeO_2(111)$ surface (Fig. 1). For an isolated single Ni atom, different adsorption sites can be explored, namely on-top of an O

anion, on the bridge between two O anions, or in the hollow position, where Ni atom adsorbs on a hollow site coordinated to three surface O anions. The later has been found to be the most stable configuration [17]. Nickel can also be deposited in small clusters. A Ni_4 three-dimensional pyramidal cluster is the most stable geometry in gas phase, closely followed by a planar rhombohedral structure [30,31]. We examined Ni deposition on a hollow site as well as both Ni_4 structures.

3.1. Ni Hollow

The interaction of an isolated Ni species on the $CeO_2(111)$ surface led to Ni adsorption on a hollow position. In our slab, the Ni atom was placed occupying the hole in the center of a triangle enclosed by O2, O4 y O8, as shown in Fig. 2. The computed adsorption energy for this configuration was $\Delta E_{ads,Ni}$ = -3.95 eV. The distance between Ni and the nearest neighbor O anions was 1.89 Å.

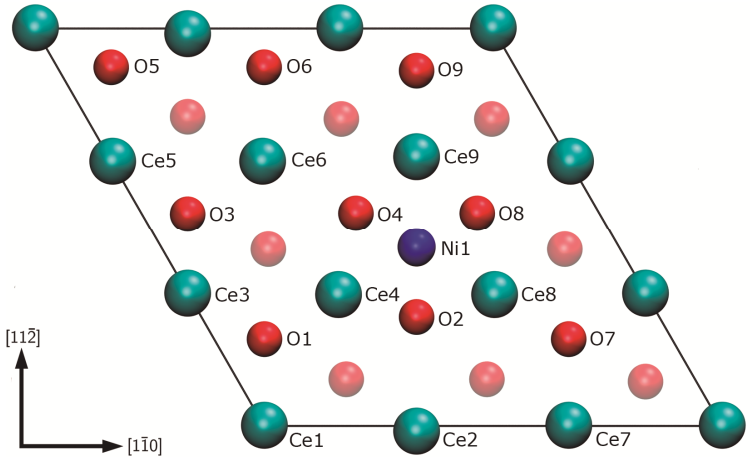

Figure 2. Front view of the $Ni_{Hollow}/CeO_2(111)$ slab

Bader charge analysis (see Table 1) indicated 8.9e for Ni, with a spin magnetization of 1.41 μB. Similar values of 8.9e and 1.2 μB where observed for Ni^{2+} ions in the NiO(100) surface [32]. Therefore, the Ni ion was characterized as Ni^{2+}.

When nickel becomes oxidized to Ni^{2+} due to its adsorption on a hollow site, two Ni(4s) electrons are transferred to the Ce(4f) band, leading to the reduction of two Ce cations. Accordingly, Bader charge analysis shows 9.9e for Ce5 and Ce6, with spin magnetizations of 1.0 μB, values corresponding to Ce^{3+} cations.

Our calculations indicate that an isolated Ni species adsorbs on the $CeO_2(111)$ surface as Ni^{2+}, and are in good agreement with the results of other theoretical and experimental works [15–17]. Particularly, our finding is consistent with that obtained from experimental measurements at low Ni coverages, which show that the electronic properties of Ni measured by Ni2p XPS and valence band UPS spectra are consistent with the formation of Ni^{2+} species [17].

Table 1. Bader charge and spin magnetization for selected ions.

System	Ion	Bader Charge (e)	Spin Magnetization (B)	Estimated Oxidation State
NiO (Ref. [32])	Ni	8.9	1.2	+2
Ni (bulk)	Ni	10.0	0.6	0
$Ni_{Hollow}/CeO_2(111)$	Ni	8.9	1.4	+2
	Ce5	9.9	1.0	+3
	Ce6	9.9	1.0	+3
	O2	7.2	0.2	-2
	O4	7.2	0.2	-2
	O8	7.2	0.2	-2
$Ni_{Pyr}/CeO_2(111)$	Ni1	9.7		+1
	Ni2	9.7		+1
	Ni3	9.7		+1
	Ni4	10.0	0.6	0
	Ce8	9.9	0.9	+3
	Ce9	9.9	0.9	+3
$Ni_{Rhom}/CeO_2(111)$	Ni1	9.7	1.0	+1
	Ni2	9.6	1.0	+1
	Ni3	9.6	1.0	+1
	Ni4	9.7	1.1	+1
	Ce1	9.8	-0.7	+3
	Ce2	9.8	-0.9	+3
	Ce8	9.9	-0.9	+3
	O1	7.2	0.1	-2
	O2	7.2	0.1	-2
	O3	7.2	0.1	-2
	O4	7.2	0.1	-2

3.2. Pyramidal Ni_4 cluster

Figure 3 shows the optimized geometrical configuration of the pyramidal Ni_4 cluster. The four Ni atoms are arranged in a pyramidal configuration with a Ni-Ni bond length of 2.30 Å, similar to the one reported in the literature for the cluster in vacuum [15]. The three Ni atoms closest to the surface form a triangle (Fig. 3) and are at 1.80 Å from O2, O4 and O8; while the other Ni atom locates in the center of this triangle, but considerably further from the surface. For this Ni_4 cluster in pyramidal structure, we computed an adsorption energy of -6.01 eV (-1.50 eV/Ni atom).

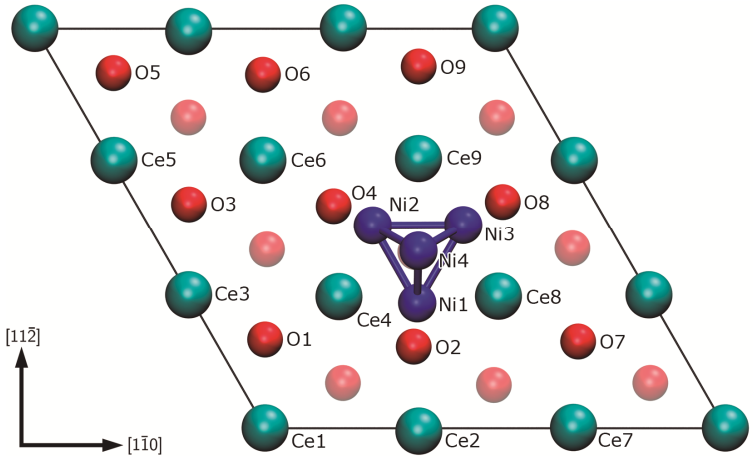

Figure 3. Front view of the $Ni_{Pyr}/CeO_2(111)$ slab

Bader charge analysis (Table 1) indicates 9.7e for Ni1, Ni2 and Ni3, which are the Ni ions closer to the surface. This value is higher than the 8.9e computed for Ni^{2+}, and comparable to that of 9.43e reported for Ni^{+1} in Ni-doped tetrahedrite [33]. So, this suggests that Ni1, Ni2 and Ni3 cations could be like Ni^{+1}. For Ni4, the upper nickel atom of the pyramid, Bader charge was instead computed in 10.0e. So, Ni4 can be considered as metallic Ni^0 atom. This configuration suggests that there is a weakening in the strength of the nickel–ceria interactions when Ni is not in direct contact with the oxide support.

On the other hand, when we examine the electronic configuration of Ce cations, only two of them (Ce8 and Ce9) are clearly reduced. In fact, the charge density difference plot shows some electronic charge is located in the hole between the Ni and the nearest O ions. This charge delocalization of Ni has been previously observed in the non-stoichiometric NiO(100) slab [33]. In this system, when an oxygen vacancy is generated in the NiO(111) surface, the electrons left behind are not localized neither on Ni nor on O. Instead, those electrons stay in the hole in between Ni and O ions.

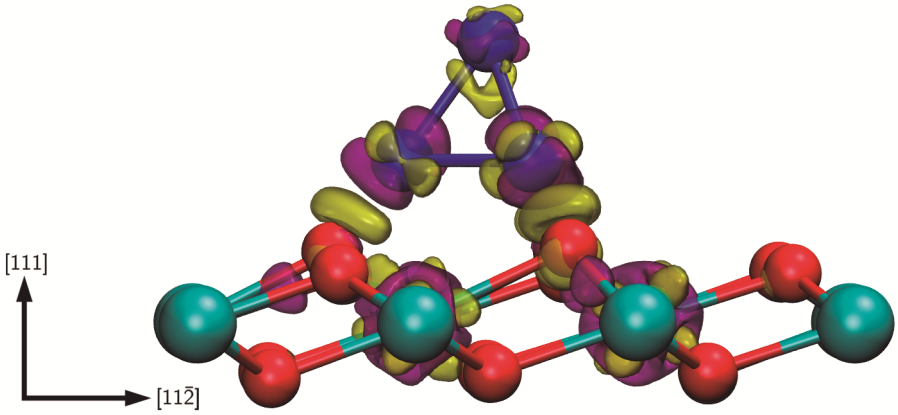

Figure 4. $Ni_{Pyr}/CeO_2(111)$. Charge density difference. The region of charge accumulation (isovalue +0.017) is presented in yellow, and that of electron depletion (isovalue −0.017) in purple.

3.3. Rhomboidal Ni_4 cluster

Figure 5 shows the optimized geometrical configuration of the rhomboidal Ni_4 cluster. In this case, the four Ni atoms are arranged in a rhomboidal structure on the ceria surface. The Ni-Ni bonds length was computed in 2.33 Å, similar to the 2.30 Å reported in other works [34]. The Ni atoms are lined up with O1, O2, O3 and O4, each of the 1.80 Å away from the nearest oxygen anion (see Fig. 5). For this configuration, we computed an adsorption energy of -6.44 eV (-1.61 eV for each Ni atom).

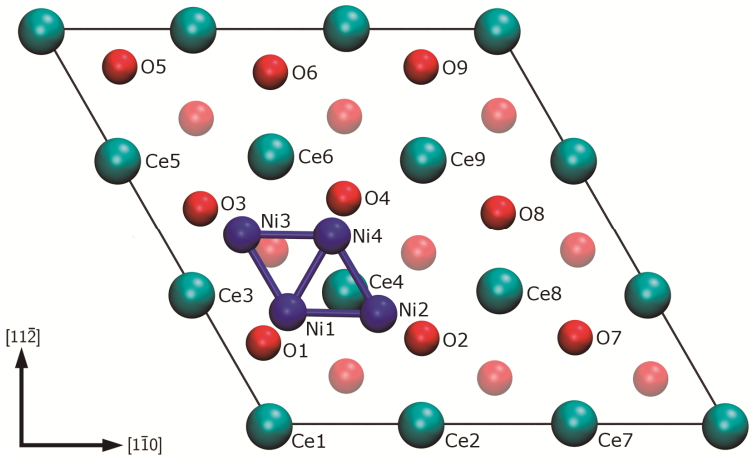

Figure 5. Front view of the $Ni_{Rhom}/CeO_2(111)$ slab.

Bader charge analysis indicates about 9.7e for all nickel ions, **comparable to that of** 9.43e reported for Ni^{+1} in Ni-doped tetrahedrite [33]. So, **this suggests that** the Ni cations **could be like** Ni^{+1}. This time we only can identify three Ce^{3+} cations (Ce1, Ce2 and Ce8), which Bader charge and spin magnetization values are reported in Table 1. The remaining electron density is located in the hole between the Ni ions and the surrounding O anions (Fig. 6), similar to what happened in the pyramidal cluster.

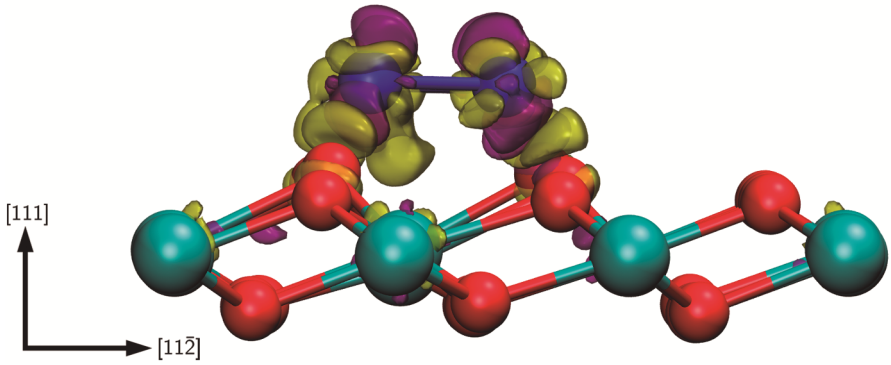

Figure 6. $Ni_{Rhom}/CeO_2(111)$. Charge density difference. The region of charge accumulation (isovalue +0.017) is presented in yellow, and that of electron depletion (isovalue −0.017) in purple.

4. Conclusions

Our DFT+U calculations have revealed strong interactions between the Ni active phase and the ceria surface, which modify the electronic properties of the ceria support and can drive the performance of Ni/CeO_2 catalysts. The interaction of an isolated Ni on the $CeO_2(111)$ surface (Ni adsorption on a hollow site) resulted in the formation of a Ni^{2+} and two Ce^{3+} species. Regarding the formation of Ni_4 clusters, the computed adsorption energy values indicate that the rhomboidal configuration is 0.43 eV more stable that the pyramidal one. Although both Ni_4 configurations show similar **Ni species**, in the pyramidal cluster the uppermost Ni atom is stabilized as Ni^0, suggesting that metal–oxide interactions are stronger for the first Ni layer. Besides, a noticeable delocalization of the charge density was observed in both Ni_4 clusters. The charge transferred by Ni oxidation is not completely localized on the Ce cations and, similarly to what was observed for the O-defective NiO(100) surface, some electron density remains in the hole between Ni and O anions. These findings provide better understanding of the $Ni\text{-}CeO_2$ interphase behavior and can help to advance the development of ceria-based supports for Ni active phase with improved catalytic performance.

Acknowledgements

The authors acknowledge the Universidad de Buenos Aires (UBACyT-20020150100095BA) and ANPCyT (FONCYT-PICT-2013-0573) for their financial support.

References

[1] J. N. Armor. Appl. Catal. A Gen. **1999**, 176 (2), 159-176.

[2] M. Balat, Int. J. Hydrogen Energy **2008**, 33, 4013-4029.

[3] H. Balat, E. Kirtay, Int. J. Hydrogen Energy **2010**, 35, 7416-7426.

[4] K. Sato, K. Fujimoto. Catal. Commun. **2007**, 8 (11), 1697-1701.

[5] B. C. Enger, R. Lødeng, J. Walmsley, A. Holmen. Appl. Catal. A Gen. **2010**, 383 (1–2), 119–127.

[6] A. Van Der Drift, J. Van Doorn, J. W. Vermeulen. Biomass and Bioenergy **2001**, 20 (1), 45–56.

[7] R. M. Navarro, M. A. Pena, J. L. G. Fierro, Chem. Rev. **2007**, 107, 3952-3991.

[8] A. Purnomo, S. Gallardo, L. Abella, C. Salim, H. Hinode, React. Kinet. Catal. Lett. **2008**, 95, 213-220.

[9] S. Xu, X. Yan, X. Wang, Fuel **2006**, 85, 2243-2247.

[10] F. B. Passos, E. R. De Oliveira, L. V. Mattos, F. B. Noronha, Catal. Today **2005**, 101, 23-30.

[11] Y. Zhou, J. Zhou. J. Phys. Chem. C **2012**, 116 (17), 9544–9549.

[12] Z. Chafi, N. Ouafek, E. Boudjennad, N. Keghouche, C. Minot, Sciences & Technologie A **2010**, 32, 15-20.

[13] D. García Pintos, Tesis doctoral: Estudio de materiales basados en óxidos de cerio usando cálculos mecano-cuánticos DFT, Facultad de Ingeniería, Universidad de Buenos Aires, **2014**.

[14] D. Xianjun, Z. Dengsong, S. Liyi, G. Ruihua, Z. Jianping, J. Phys. Chem. C **2012**, 116, 10009−10016.

[15] Y. Zhou, J. M. Perket, A. B. Crooks, J. Zhou. J. Phys. Chem. Lett. **2010**, 1 (9), 1447–1453.

[16] S. D. Senanayake, J. Evans, S. Agnoli, L. Barrio, T. L. Chen, J. Hrbek, J. A. Rodriguez. Top. Catal. **2011**, 54 (1–4), 34–41.

[17] J. Carrasco, L. Barrio, P. Liu, J. A. Rodriguez, M. V. Ganduglia-Pirovano. J. Phys. Chem. C **2013**, 117 (16), 8241–8250.

[18] L. Eyring, Handbook on the Physics and Chemistry of Rare Earths, in: K.A. Gschneider, L. Eyring (Eds.), North-Holland, Amsterdam, **1979**.

[19] J.C. Conesa, Surf. Sci. 1995, 339, 337–352.

[20] M. Nolan, S. Grigoleit, D.C. Sayle, S.C. Parker, G.W. Watson, Surf. Sci. **2005**, 576, 217–229.

[21] N.V. Skorodumova, M. Baudin, K. Hermansson, Phys. Rev. B **2004**, 69, 075401.

[22] G. Kresse, J. Furthmuller, Comp. Mat. Sci. **1996**, 6, 15.

[23] G. Kresse, J. Hafner, J. Phys. Rev. B: Cond. Matt. Mat. Phys. **1993**, 47, 558.

[24] H. Monkhorst, J. Pack, Phys. Rev. B **1976**, 13, 5188–5192.

[25] M. Nolan, S. C. Parker, G. W. Watson, Surf. Sci. **2005**, 595, 223-232.

[26] C. W. M. Castleton, J. Kullgren, K. Hermansson. J. Chem. Phys. **2007**, 127 (24).

[27] R. F. W. Bader. Chem. Rev. **1991**, 91 (5), 893-928.

[28] W. Tang, E. Sanville, G. Henkelman. J. Phys. Condens. Matter **2009**, 21 (8), 84204.

[29] G. Henkelman, A. Arnaldsson, H. Jónsson, Comput. Mater. Sci. **2006**, 36, 354-360.

[30] F. A. Reuse, S. N. Khanna. Chem. Phys. Lett. **1995**, 234 (1–3), 77–81.

[31] Q. L. Lu, Q. Q. Luo, L. L. Chen, J. G. Wan. Eur. Phys. J. D **2011**, 61 (2), 389–396.

[32] A. M. Ferrari, C. Pisani, F. Cinquini, L. Giordano, G. Pacchioni. J. Chem. Phys. **2007**, 127 (17), 174711.

[33] X. Lu, D. T. Morelli, Y. Xia, V. Ozolins. Chem. Mater. **2015**, 27 (2), 408–413.

[34] G. Schmid, Clusters and Colloids: From Theory to Applications, VCH, Weinheim, **1994**.